A Robust Titanium Isophthalate Metal-Organic Framework for Visible-Light Photocatalytic CO2 Methanation

Sujing Wang, María Cabrero-Antonino, Sergio Navalón, Chen-chen Cao, Antoine Tissot, Iurii Dovgaliuk, Jérôme Marrot, Charlotte Martineau-Corcos, Liang Yu, Hao Wang, et al.

A Robust Titanium Isophthalate Metal-Organic Framework for Visible Light Photocatalytic CO_2 Methanation

Sujing Wang[1,2,8]*, Maria Cabrero-Antonino[3], Sergio Navalón[3], Chen-chen Cao[1], Antoine Tissot[1], Iurii Dovgaliuk[1], Jérôme Marrot[4], Charlotte Martineau-Corcos[4,5], Liang Yu[6], Hao Wang[6], William Shepard[7], Hermenegildo García[3]*, Christian Serre[1]*

[1]Institut des Matériaux Poreux de Paris, UMR 8004 CNRS, Ecole Normale Supérieure, Ecole Supérieure de Physique et de Chimie Industrielles de Paris, Université PSL, 75005 Paris, France

[2]Hefei National Laboratory for Physical Sciences at the Microscale, University of Science and Technology of China, 230026, Hefei, China

[3]Departamento de Química, Universitat Politècnica de València, 46022, Valencia, Spain

[4]Institut Lavoisier de Versailles, UMR 8180 CNRS, Université de Versailles Saint-Quentin-en-Yvelines, Université Paris-Saclay, 78035 Versailles, France

[5]CEMHTI, UPR 3079 CNRS, 45071 Orléans CEDEX 2, France

[6] Hoffmann Institute of Advanced Materials, Shenzhen Polytechnic, Shenzhen 518055, Guangdong, China

[7]Synchrotron SOLEIL, L'Orme des Merisiers, Saint-Aubin, BP 48, 91192, Gif-Sur-Yvette, France

[8]Lead contact

*E-mail: sjwang4@ustc.edu.cn

hgarcia@qim.upv.es

christian.serre@ens.fr

SUMMARY

Isophthalic acid (IPA), a feedstock linker, has been considered so far to build series of topical metal-organic frameworks (MOFs) of diverse structures with various di- and trivalent metal ions, such as CAU-10(Al), owing to its facile availability, unique connection angle/mode and a wide scope of functional groups attached. Constructing MOFs from IPA and tetravalent metals, typically Group 4 metals, would be of a great interest due to expected higher chemical stability. In particular, titanium-IPA frameworks possessing photoresponse is alluring, in relation to the known challenge of synthesizing new Ti-MOFs. Here, we have synthesized the first Ti-IPA MOF, denoted as MIP-208, via a solvothermal process that efficiently combines the use of preformed Ti_8 oxoclusters and *in situ* acetylation of 5-NH_2-IPA linker. MIP-208 has helical chains of *cis*-connected corner-sharing TiO_6 polyhedra as the inorganic building units, which are interconnected to each other leading to a 3D ultramicroporous framework. Solid-solution mixed linkers strategy was then successfully applied resulting in a series of multivariate MIP-208 structures with tunable chemical environment and sizable porosity. Finally, the excellent thermal and hydrolytic stabilities of MIP-208 allowed its use for the photocatalytic carbon dioxide (CO_2) methanation, showing the best result among the pure MOF catalysts. Ruthenium oxide nanoparticles were further photodeposited on MIP-208 forming a highly active and selective composite catalyst, MIP-208@RuO_x, to largely improve the photocatalytic performance, which features a notable visible light response, an excellent stability and recycling ability.

INTRODUCTION

Metal-organic frameworks (MOFs) or porous coordination polymers (PCPs) have been recognized as one of the most intensively investigated heterogeneous catalysts for liquid phase reactions, due to their porous tunable structure, high surface area, and acidic/basic sites or metal nodes with versatile and spatially controlled distribution.[1-3] Organic ligand plays an essential role in the formation of the MOF structure and introduction of corresponding property.[4; 5] As organic synthesis evolved significantly during past decades, almost unlimited organic compounds have been applied in the MOF fabrication via the linker-engineering strategy, resulting in a vast combination of structures and functions.[6-8] However, time and effort requiring organic synthesis for linker preparation undoubtedly limits the reproduction and application of costly MOF candidates.[9; 10] In this regard, commercially available organic linkers from industry are of great interests due to their easy availability at large scale and low cost.[11; 12]

Benzene-dicarboxylic acid isomers are representative compounds fulfill the aforementioned demand currently produced in billion-kilogram scale annually. The three isomers, namely *ortho*-phthalic acid (phthalic acid), *meta*-phthalic acid (isophthalic acid, IPA) and *para*-phthalic acid (terephthalic acid), are all important feedstock for preparation of a large number of industrial products.[13; 14] In their use of constructing MOFs, phthalic acid alone tends to form materials of low dimensionality, mainly due to the deficient separation and steric hindrance between the adjacent carboxylate groups.[15-17] On the contrary, terephthalic acid is one of the most popular carboxylate linkers from the very beginning of the MOF journey.[18] The ideal configuration with suitable molecular length, perfect separation of coordination sites and varied connection modes make it adaptable to MOF structures with any dimension built with almost every sort of metal element.[19-21]

In the case of isophthalic acid, the unique angle (120°) and the medium distance between the two carboxylate groups enable a large degree of manipulation in synthesizing MOFs compared with the other two isomers. Numerous metal-IPA

frameworks have been identified with nodes ranging from alkaline earth[22], to divalent and trivalent transition metals[23-26], as well as rare earth[27-29] or main group elements[30-32], and even mixed metal systems[33-35], in which the *meta*-side of the coordinated carboxylate groups on the benzene ring frequently faces the structure void. IPA offers thus an obvious and facile opportunity of tuning the chemical environment of the MOF pore via introduction of functional groups on the *meta*-side. Correspondingly, distinct organic functions on the 5- and 4-position of the benzene ring have been presented in the reported examples, showing great interests and potential in fine-tuning the structure-property correlation[36-39].

It is noteworthy that isophthalic acid is compatible for the MOF assembly with every transition metal subgroup but not the Group 4 elements in the periodic table, which indicates, to the best of our knowledge, no report of IPA based-MOF example built with titanium (Ti), zirconium (Zr), hafnium (Hf) or rutherfordium (Rf). On the other hand, Ti and Zr, the most common Group 4 metals, have attracted major attention of the MOF research community during the past years, owing to their high natural abundances, low toxicities, strong interactions with oxygen sites and thus significantly enhanced stabilities once in the MOF structures.[40; 41]

More recently, the potential of MOFs has been expanded to other areas of catalysis, particularly in photocatalysis.[42] The strong interaction between the positively charged metal nodes and negatively charged antenna linkers in rigid configurations makes MOFs suitable in promoting photoinduced charge separation.[42] Hence, an electron transfer from the organic linker in its excited state to the metal node upon light absorption appears a general photochemical step, especially in the case of a favorable overlapping between the lowest occupied crystal orbit (LOCO) with the atomic orbitals of the metal cations.[43] For this reason, MOFs are among the most promising porous photocatalysts, particularly for the production of solar fuels.

Taking into account the prevalent role that MOFs and derivative materials in photocatalysis, Ti-MOFs have attracted considerable attention due to the known

activity of TiO_2 and Ti-oxo clusters to undergo photoinduced charge separation.[44] In general, Ti-MOFs are not only promising candidates as photo-responsive materials,[45] but also show great potential in gas separation,[46; 47] proton conduction[48] and clinical applications.[49] Nevertheless, direct synthesis of Ti-MOFs still remains an important challenge,[50] despite the gradually increased number of reported Ti-MOF structures over the past decade, in most of the cases attained through serendipity. It is admitted that an infinite number of Ti-O units is expected to facilitate photoinduced charge separation and charge mobility, in comparison with MOFs based on discrete inorganic units with a low number of Ti-O bonds. One and two dimensional (1D and 2D) arrays of Ti-O units should thus in principle improve the semiconducting properties of the Ti-MOFs.[51] In this context, the photoactive Ti-MOFs that have been prepared so far are those with 1D chain or nanowire of Ti-O building units, whose photo-responsive behaviors have been proven to be closer than those compounds constructed of discrete Ti-O clusters to that of bulk TiO_2.[52] As shown in Figure 1, there are only three kinds of 1D Ti-O inorganic building units reported up to date, namely the TiO chains in MIL-91,[53] the Ti_6O_9 nanowires in MIP-177-HT,[52] ZSTU-1, 2 and 3,[54] and the TiO chain in DGIST-1.[55] Therefore, as these MOFs are all constructed from sophisticated ligands, it would be of great interest to discover IPA type linker-based Ti-MOFs with infinite Ti-O building units. It would not only expand the scope of Ti-MOFs structural and chemical diversity, but also might lead to improved photocatalytic performance.

Herein, we report an ultramicroporous Ti-MOF, denoted as MIP-208 (MIP stands for the Materials of the Institute of porous materials from Paris), the first MOF composed of Group 4 metal and IPA type linker. In the crystal structure of MIP-208, helical chains of cis-connected corner-sharing TiO_6 polyhedra are held in place by the *in situ* generated 5-acetamidoisophthalate (5-Aa-IPA) linker molecules, giving rise to a 3D framework with 1D channel-like accessible voids running along the *c*-axis. Benefiting from their shared structural configuration and coordination adaptability, mixed linker of 5-Aa-IPA and other IPA derivatives having diverse functional groups on the meta-position of the carboxylate groups could further be introduced in the framework

following a solid-solution strategy, resulting in a series of multivariate MIP-208 structures. Furthermore, the dual presence of amide group and the 1D TiO chain unit in the porous structure of MIP-208 associated with an excellent thermal and hydrothermal stability has allowed developing a photocatalyst for carbon dioxide (CO_2) methanation based on RuO_x nanoparticles (NPs) with visible light photoresponse, reaching at 200 °C a productivity of 0.8 mmol $g_{catalyst}^{-1}$ in 22 h.

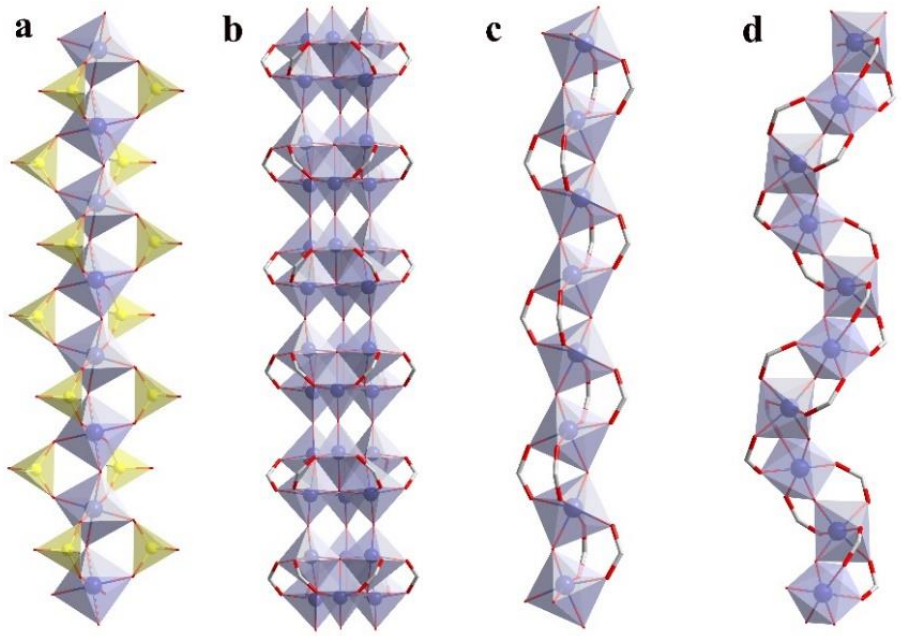

Figure 1. Comparison of 1D Ti-O inorganic building units reported. a) Linear TiO chain in MIL-91. b) Linear Ti_6O_9 nanowire in MIP-177-HT, ZSTU-1, 2 and 3. c) Linear TiO chain in DGIST-1. d) Helical TiO chain in MIP-208 reported here.

RESULTS AND DISCUSSION

Twenty-four different Ti-MOFs prepared from direct-synthesis have been reported to date. The Ti sources used to produce these MOFs can be classified into two kinds: simple Ti complexes and polynuclear TiO clusters. Compared with simple Ti complexes, such as $TiCl_3$, $TiCl_4$, and $Ti(iPrO)_4$, Ti-oxoclusters are known to slow down the reaction rate and avoid the undesirable hydrolytic formation of TiO_2, owing to the gradual Ti-O connection rearrangements of the oxocluster precursor for most cases. Thus, it usually leads to highly crystalline Ti-MOF materials constituted by

large single crystals.[55-57] In this regard, a Ti_8O_8 cluster with formate and acetate terminals (Ti_8AF) was selected here, due to its facile preparation, easy handle, suitable stability and reactivity.[58] Regarding the reaction solvent, it is well-recognized that the conventional ones, such as dimethylformamide (DMF) and diethylformamide (DEF), should be replaced by greener solvents to decrease the toxicity and harm to human and environment. Based on our previous success of preparing Group 4 metal MOFs, formic acid, acetic acid and acetic anhydride, which have been shown to efficiently slow down the reaction leading to highly crystalline products, were selected as solvents. 5-NH_2-IPA was selected as the linker due to the documented benefit of the amino group presence in increasing the CO_2 adsorption and enhancing visible light photoresponse.[59; 60]

Initial reaction attempts indicated that the aforementioned three acidic solvents can interfere with decomposition of the Ti_8AF precursor, while offer a good solubility to the 5-NH_2-IPA linker. However, all attempts did not generate any crystalline solid. Various additives known to either facilitate the linker exchange or promote the Ti-O connection rearrangement were tested, such as water, methanol, ethanol, acetone, and DMF. A highly crystalline product of a dark yellow or light brown color was formed only when methanol was used in the mixture of acetic acid and acetic anhydride. Acetic acid was found to be not necessary for the product formation, but to accelerate the reaction rate. An *in situ* amidation took place between the amino group of 5-NH_2-IPA and acetic anhydride, generating the 5-acetamide-IPA (5-Aa-IPA) as the final framework building linker (Figure S1). Solid state NMR data collected on the as-synthesized MIP-208 sample demonstrated the presence of 5-Aa-IPA within the structure (Figures S2 and S3).

It is likely that the *in situ* acetylation step is critical to yield the crystalline material, which possibly slows down the reaction rate significantly. A control experiment using the preformed 5-Aa-IPA as linker under the same reaction conditions did not lead to MIP-208, but to an amorphous solid. Therefore, this solvothermal synthesis is likely

to benefit synergistically from the rearrangement of the Ti_8AF cluster and *in situ* linker formation, which is a rare case for MOF preparation reported so far. However, it could provide us a valuable and even possibly rational strategy for further synthesizing new Ti-MOFs through a control of the reaction rate from both inorganic and organic precursor conversions.

MIP-208 was obtained as microsize single crystals, ruling out its structure determination from laboratory diffraction. Thus Synchrotron diffraction single-crystal data of MIP-208 was collected with a microfocused X-ray equipment on the Proxima 2A beamline (Synchrotron SOLEIL, France)[61] to determine its crystal structure. The coordination environment of Ti^{4+} ion and the overall framework connection could be solved precisely, despite that the accurate position of the acetamide group could not be located due to its disorder. Assisted by the solid-state NMR characterization, a formula of Ti(μ_2-O)(5-Aa-IPA) could be concluded for MIP-208. It crystallizes in tetragonal $I4_1/amd$ space group (No. 141), associated with unit-cell parameters of a = b = 21.8190 Å, and c = 10.9380 Å. As shown in Figure 2a, each Ti^{4+} ion is in an octahedral coordination geometry with four carboxylate oxygen atoms and two μ_2-O oxo groups. The adjacent TiO_6 polyhedra adopt a cis-connected corner-sharing mode to connect each other, giving rise to a 1D infinite chain secondary building unit (SBU) running along the c-axis. Unlike the linear 1D Ti-O SBUs in MIL-91,[53] DGIST-1[55] and MIP-177-HT,[52] the helical TiO chain in MIP-208 is the first example of this type of SBU observed in Ti-MOFs, to our knowledge (Figure 1). Al(OH) chain with similar configuration was discovered previously in the CAU-10 MOF series (CAU stands for Christian-Albrechts-University),[62] with μ_2-OH group as the sharing-corner. Notably, the replacement of bridging OH in trivalent metal-based MOFs by oxo group in similar MOFs built with tetravalent metal could lead to a dramatic difference in terms of structural flexibility and related properties, as documented in MIL-47 and MIL-53 compounds (MIL stands for Materials from Institute Lavoisier).[63; 64] In particular, the presence of OH or oxo groups in Ti-O materials has been demonstrated to be critical to their performance in photocatalysis,[65-67] which highlights the

importance of TiO chains in MIP-208 structure over its analogues with the lower valence metal ions.

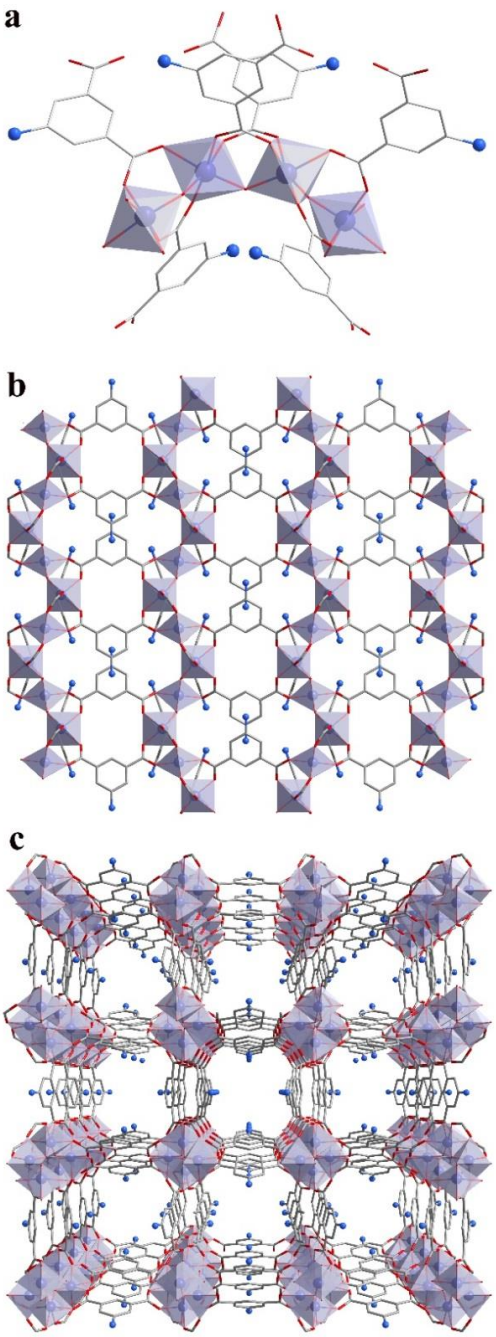

Figure 2. Crystal structure of MIP-208 : (a) Coordination environment of Ti^{4+} ion and arrangement of 5-Aa-IPA linkers around it. (b) along the *b*-axis. (c) along the *c*-axis, showing 1D channels (Ti in purple, C in gray, O in red, the blue ball stands for the acetamide group, all hydrogen atoms are omitted for clarity).

The neighboring TiO chains are interconnected via pairs of 5-Aa-IPA linkers in an up and down mode to avoid as much as possible the steric hindrance (Figure 2b), resulting in a 3D framework with double-walled 1D channels running along the *c*-axis (Figure 2c). One can expect its micropores to be accessible for guest molecules as reported before for CAU-10 compounds constructed from IPA bearing the bulkiest functional groups,[62; 68] due to large size and thus considerable steric hindrance of the acetamide groups facing the pores. As reported before for CAU-10-OMe and CAU-10-Br, MIP-208 did not show any accessibility for nitrogen at 77 K, but a noticeable porosity for CO_2 (Figure S4).

A large number of functionalized IPAs are commercially available chemicals offered at low prices. The good compatibility of IPA derivatives regarding their behavior in coordination chemistry has been documented,[37] thus offering a great promise to tune the chemical environment of the pore in MIP-208 structure via a solid-solution mixed linkers strategy. Solid-solution strategy is a powerful alternative way to introduce multiple functional groups together in the MOF structures, especially when the direct synthesis of isostructural MOF built with a single linker bearing specific functional group is challenging.[69-71] This strategy suits perfectly the case of MIP-208, since all attempts to directly synthesize the corresponding MIP-208 analogues using other functionalized IPAs instead of 5-NH_2-IPA failed, resulting in either amorphous solids or crystalline phases of different structures. Therefore, mixed linkers were considered via one-pot reactions to prepare series of multivariate MIP-208s (MTV-MIP-208, Figure 3a). Several representative IPA type dicarboxylic acids, including IPA, 5-NO_2-IPA, 5-Me-IPA, 5-Br-IPA, 5-tBu-IPA, 3,5-pyrazole-dicarboxylic acid (PDA) and camphoric acid, were selected as the substitution linkers, aiming to replace the 5-Aa-IPA spacer in the MIP-208 framework. All the tested linkers except for 5-NO_2-IPA and camphoric acid could reach certain substitution ratios, ranging from 11 mol% to 50 mol% (Figure S5), as deduced from the NMR data. However, the reason for the unsuccessful inclusion of 5-NO_2-IPA and camphoric acid is not clear yet and still under investigation.

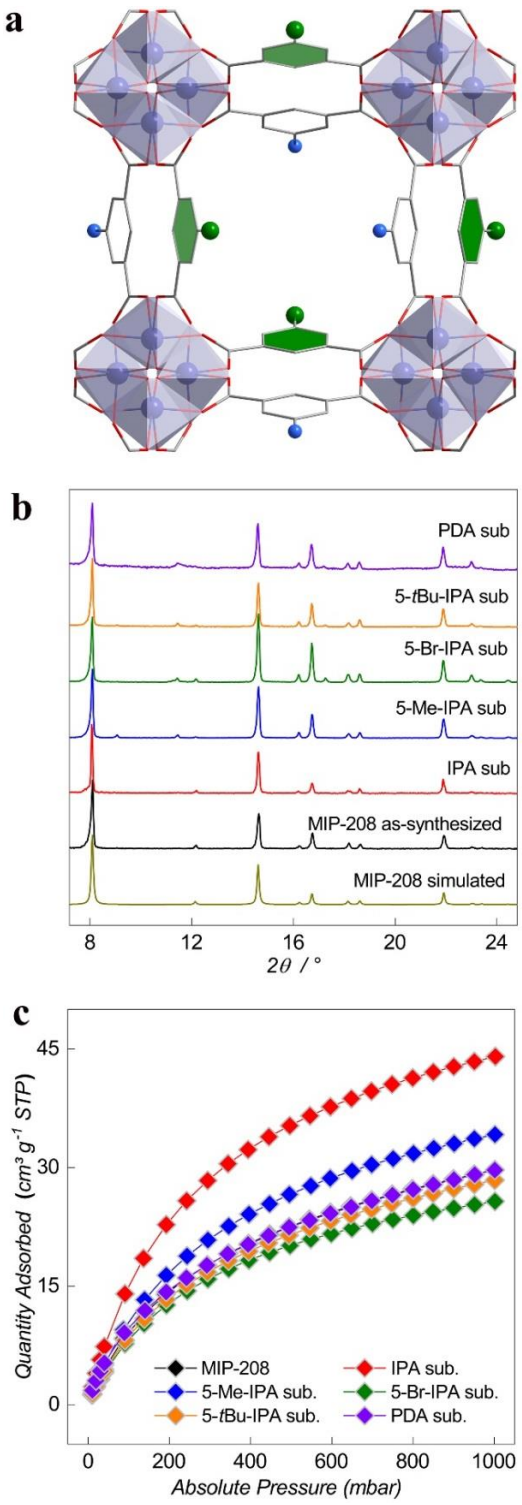

Figure 3. Illustration and characterizations of MTV-MIP-208 materials. (a) Illustration of MTV-MIP-208 structure with multiple functional groups (the blue ball stands for the acetamide group, the green ball stands for the other functional groups, and all hydrogen atoms are omitted for clarity) (b) PXRD patterns of the parent and MTV-MIP-208s (λ_{Cu}≈1.5406 Å). (c) CO_2 adsorption isotherms collected at 273 K for parent and MTV-MIP-208 solids.

As shown in Figure 3b, the inclusion of the second linker did not generate noticeable changes on the overall structural long-range order, as evidenced by their highly similar PXRD patterns. On the contrary, the porosity of the resulting materials was altered, as deduced from the CO_2 adsorption isotherms collected at 273 K (Figure 3c). For instance, the sample with 50 mol% IPA substitution ratio led to a significant enhancement of CO_2 uptake (50% at both 0.15 and 1 bar) compared with the pure MIP-208, likely due to the much less steric hindrance of lighter H over the acetamide group. A similar observation was noticed for the 5-Me-IPA mixed sample (33 mol%). In the case of 5-Br-IPA derivative (38 mol%), a slight decrease of uptake in comparison with the parent compound has been observed, probably attributable to a much larger atomic weight of Br atom, in spite of its lower steric hindrance. When the slightly bulkier *t*Bu group but with similar molecular weight was introduced to replace the acetamide one, the sample shows limited drop in pore volume mainly due to the small linker substitution ratio (17 mol%). It is worth noting that even PDA, which has a five-membered heterocyclic aromatic moiety, could be included in the MIP-208 framework, though the substitution ratio is low (11 mol%), probably due to the similar angle of the two carboxylate groups and the presence of basic N-site on the heterocyclic ring. Therefore, solid-solution strategy is here an efficient way to expand and modify the chemical variety of the MIP-208 structural cavity, leading to a series of MTV-MIP-208 materials.

Stability of MOF is a practical concern in applications. For instance, photocatalytic methanation requires a combination of good thermal, hydrolytic and UV irradiation stability of the MOF catalyst, since the catalysis is normally carried out at a temperature close to 200 °C, under UV irradiation and in the presence of generating stoichiometric water as the side product. Therefore, the stability of MIP-208 was tested before applying it to the photocatalytic methanation. The results from both temperature-dependent PXRD measurement and thermogravimetric analysis (TGA) support the high stability of MIP-208 (Figure S6). Its ordered crystal structure is stable up to 325 °C in air, which is comparable to MIP-177-HT, and clearly surpass

MIL-91 and DGIST-1 (unstable above 200 °C). Furthermore, the activated MIP-208 sample hardly adsorb water when exposed in air for a long time (less than 5%), considerably much less than the Al-CAU-10 series do. This enhanced hydrophobicity of MIP-208 is thus associated to the bridging oxo group effect, in comparison with the OH in CAU-10, as well as the limited hydrophilic character of acetamide.

Hydrolytic stability of MIP-208 was tested by soaking it in liquid water at room temperature for three days and heating it in boiling water for 8 h separately. The PXRD patterns of the tested samples are identical to that of the as-synthesized one (Figure 4a), supporting the robustness of the crystalline long-range order. CO_2 adsorption data (Figure 4b) confirm the good hydrolytic stability of MIP-208, with minor differences between the sample before and after water treatments. It is worth noting that MIP-208 is among the most hydrothermally stable Ti-MOFs, comparable to that of the Ti-bisphosphonate MIL-91, outperforming all Ti-carboxylate MOFs reported so far.

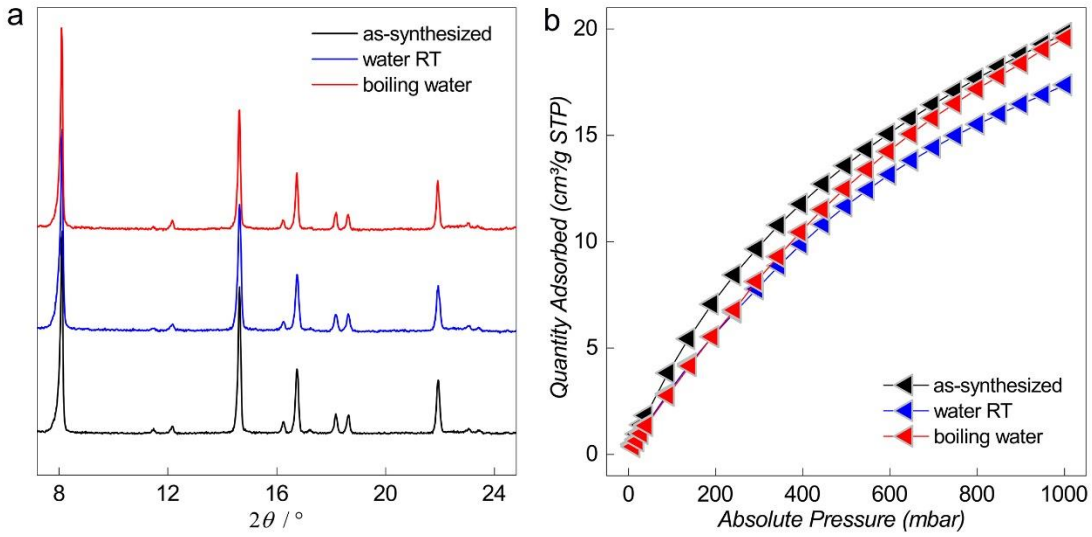

Figure 4. Results of water stability tests. (a) PXRD patterns and (b) CO_2 adsorption isotherms collected at 298 K for the MIP-208 samples before and after water treatments.

As MIP-208 possesses 1D TiO chain building block, a good photoresponsive activity is expected. Photocatalytic conversion of CO_2 to methane was thus selected as the

model reaction, since this reaction could generate value-added product from CO_2 emissions. Promising progress of using MOF-based heterogeneous catalysts for CO_2 conversion to methane has been achieved lately.[72] For instance, MOFs supported nickel and platinum nanoparticles (NPs) could promote the thermal methanation under harsh conditions, such as high pressures and temperatures. Photocatalytic methanation by MOF-based catalysts has however been hampered for a long time by the poor selectivity until the recent success reported when a HKUST-1@TiO_2 core-shell composite was applied under UV irradiation, but with rather low efficiency.[73] Lately, the first example of pure photoactive MOF towards catalytic methanation has been reported, which involves ZnO inorganic bricks in a nitrogen-rich framework exhibiting a CH_4 generation productivity of 30 μmol·$g_{catalyst}^{-1}$ after 24 h at 215 ºC under UV light irradiation. A notable enhancement of activity was attained via supporting Cu_2O NPs on the Zn-MOF to form a composite catalyst, which led to a CH_4 production of 45 μmol·$g_{catalyst}^{-1}$ under the same condition.[74] Those breakthroughs are undoubtedly encouraging. However, the photocatalytic activity of MOF materials is however very low. Thus developing efficient and selective MOF-based photocatalyst for methanation is of great interests, yet remains a challenge.

Pure MIP-208 sample was first tested for the photocatalytic methanation reaction. A CH_4 production of about 40 μmol/$g_{catalyst}^{-1}$ could be achieved using MIP-208 as the catalyst in the mixture of CO_2 (0.25 bar) and hydrogen (1.05 bar) under UV irradiation (Xenon lamp, 1350 W×m^{-2}) at 200 ºC after 22 hours (Figure S7). This result highlights the positive influence of 1D TiO chain SBU in MIP-208 regarding its photo-response, since the benchmark NH_2-MIL-125 built with discrete Ti_8 clusters exhibits negligible photocatalytic activity under similar reaction conditions.[74] Furthermore, in comparison with the state-of-the-art MOF photocatalyst for methanation,[74] an enhancement of 33 % in efficiency was noticed for MIP-208, which suggests that MIP-208 could be the most efficient pure MOF photocatalyst for methanation up to now, to our knowledge.

In order to further improve the CH_4 formation rate, incorporation of metal NPs onto MIP-208 to form a composite catalyst was considered, since it is well-documented that photocatalytic methanation generally requires the presence of a metal or metal oxide with hydrogenation activity such as nickel, copper, rhodium, palladium, or ruthenium.[75] We initially selected RuO_x NPs as the composite component, owing to the fact that Ru species generally show the highest activity in CO_2 methanation under milder conditions despite their limited selectivity compared with other active elements.[76; 77] In addition the oxide form instead of elemental metal NPs features elevated stability to facilitate easy handling during catalysis process. The MIP-208@RuO_x composite was obtained following the post-synthetic photo-deposition of RuO_x NPs on MIP-208 by photocatalytic reduction of water soluble $KRuO_4$ using methanol as sacrificial electron donor (Figure S8). The success of RuO_x photodeposition by photocatalytic perruthenate reduction evidenced further the photoactivity of MIP-208 material, as it has been proven that an evidence supporting the occurrence of photoinduced charge separation upon irradiation of a solid is the observation of photodeposition onto the material of metal NPs from aqueous solutions.[78]

After deposition, determination of the Ru content and average particle size in the composite was carried out. Energy-dispersive X-ray spectroscopy (EDX) analysis of MIP-208@RuO_x showed a Ru content of 0.76 wt%. Field emission scanning electron microscopy (FESEM) images of MIP-208@RuO_x displayed a similar crystallite morphology as that of the pristine MOF, without obvious free RuO_x particles (Figure S9). Dark-field scanning transmission electron microscopy (DF-STEM) measurements revealed the presence of small RuO_x NPs (1.4±0.14 nm). The homogeneous distribution of RuO_x NPs all over MIP-208 was further confirmed by DF-STEM coupled to an EDX detector (Figure S10).

Preservation of the crystalline structure of MIP-208 after RuO_x photodeposition was confirmed by PXRD data (Figure S11). The lack of additional peaks in the composite

pattern compared with that of the pure MIP-208 could be attributed to the low Ru loading and the evenly distributed small particle size, as determined by TEM images.

The MIP-208@RuO_x solid was also characterized by X-ray photoelectron spectroscopy (XPS, Figure S12). The C1s spectrum shows the presence of aromatic carbons (284.4 eV). In addition, a band centred at 285.9 eV attributable to the C-N bond of the amide groups is observed, together with another centred at 289 eV that can be assigned to the carbonyl of both the amide and the carboxylate groups. The amide group is clearly observed in the N1s band centred at about 399 eV as well. The broad O1s band is mainly due to the presence of oxygen atoms in the carboxylate and amide groups, together with the Ti-O and Ru-O bonds. Ti2p spectrum can be assigned to the presence of Ti^{4+} ion. Ruthenium is recognized by the bands appearing at about 280.7 and 282.4 eV that can be assigned to the Ru $3d_{5/2}$ of RuO_2 and hydrated RuO_2, respectively.[79; 80] The expected Ru $3d_{3/2}$ band appearing at higher binding energies (~4.1 eV) (Supplementary Figure 12a) is, however, difficult to observe, since it overlaps with the C-N contribution of the acetamido groups.[78; 80] XPS analysis also can provide an estimation of the valence band maximum of the MIP-208@RuO_x solid by measuring the lowest energy electron band of the material referred to the work function of the instrument. As shown in Supplementary Figure 13, a valence band potential of -1.51 eV was estimated. This value together with the 2.92 eV bandgap measured from the Tauc plot of the diffuse reflectance UV-Vis spectrum, gives a value for the LUCO of -2.874 eV.

The photocatalytic performance of the MIP-208@RuOx composite in CO_2 methanation was then evaluated under the same reaction condition as that used for testing the pristine MOF. As expected, a selective CO_2 conversion into CH_4 (800 $\mu mol/g_{catalyst}^{-1}$) as the only product was observed. Specifically, CO and C_2H_6 amounts were under the detection limit of our micro-GC. This CH_4 production value is 20 times higher compared with that obtained using the pure MIP-208 sample. Control experiments using MIP-208@RuO_x in the dark under the same reaction condition

showed negligible CH_4 production.

Similar time-conversion plot, with a slightly lower CH_4 formation rate, was also measured using simulated sunlight irradiation (1 Sun) (Figure 5a). The difference between the CH_4 production using the xenon lamp or the simulated sunlight can be attributed to the lower power of the simulated sunlight (1000 $W \times m^{-2}$) compared to the Xenon lamp (1350 $W \times m^{-2}$). This similarity in the temporal CO_2 conversion indicates that a major percentage of the MIP-208@RuO_x photoresponse must derive from the visible region. Otherwise, a more noticeable decrease in photocatalytic activity, much larger than that expected from the power ratio, should have been observed since the UV content of the simulated sunlight is very minor compared with the xenon lamp.

Cycling stability of the MIP-208@RuO_x composite as photocatalyst was determined by performing a series of consecutive reuses following the temporal evolution of CO_2 conversion and CH_4 formation. These stability tests are important considering the conditions of the photocatalytic methanation, particularly the presence of H_2O and the reaction temperature of 200 °C. The results presented in Figure 5b show coincident plots for the temporal CH_4 evolution upon seven consecutive runs, supporting the stability of the material under the conditions of the photocatalytic reaction. It is noteworthy that this highly selective and constant methanation activity promoted by RuO_x has hardly been achieved before, as CO has been proven as the side product in this reaction, which led to a considerable deactivation of the catalyst.[77] Additionally, irradiation of the composite in argon atmosphere using the Xe lamp or solar simulator at 200 ºC revealed the evolution of a tiny amount of CO_2, corresponding to the decomposition of a small fraction of the IPA linkers present in the material (<0.05 μmol CO_2/μmol ligand). This small CO_2 evolution from MIP-208@RuO_x compares favourably with the stability of the most robust MOFs reported as photocatalysts under similar irradiation conditions.[81]

The crystallinity of the MIP-208@RuO_x sample after seven times cycling in catalysis was well-maintained, as no notable change in the PXRD pattern was observed (Figure

S14). Furthermore, the solid-state ^{13}C-NMR spectra of the fresh and seven-time reused MIP-208@RuO_x were coincident (Figure S15). DF-TEM images of the catalyst after cycling were also similar to those of the fresh sample, without any evidence of RuO_x particle growth or agglomeration (Figure S16). Thus, both photocatalytic activity and characterization of the seven-times used MIP-208@RuO_x sample indicate the stability of the material under irradiation conditions.

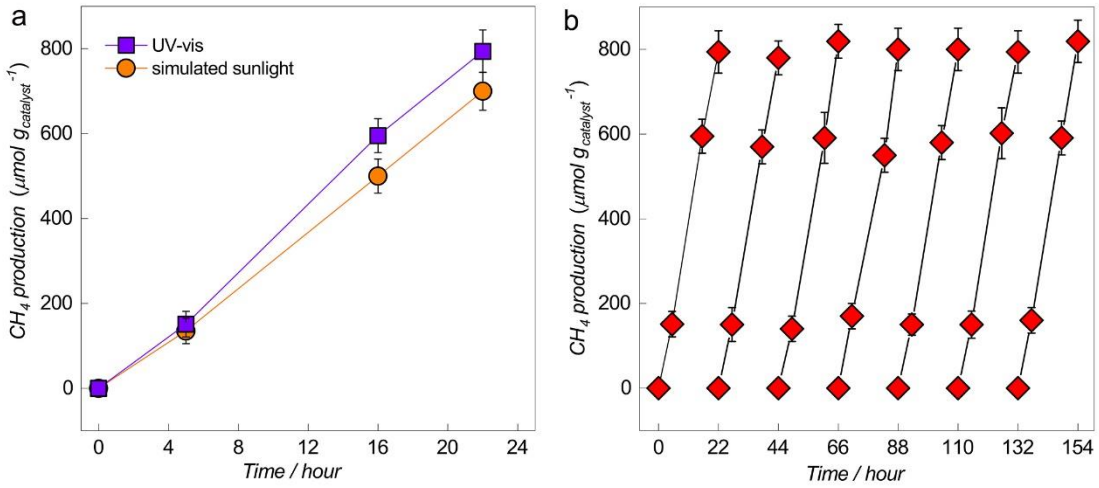

Figure 5. (a) Temporal evolution of CH_4 during the photocatalytic CO_2 reduction with MIP-208@RuO_x as the catalyst using a Xenon lamp or a solar simulator. b) Reusability of MIP-208@RuO_x in the photocatalytic CO_2 methanation (seven times cycling) using a xenon lamp as irradiation source. Reaction conditions: catalyst (15 mg), H_2 (1.05 bar), CO_2 (0.25 bar), temperature (200 ºC), irradiation source a xenon lamp (1350 W×m^{-2}) or solar simulator (1000 W×m^{-2}).

To determine the origin of CH_4, an experiment using ^{13}C-labelled CO_2 was carried out, monitoring the isotopic composition of CH_4 evolved by mass spectrometry. The results presented in Figure S17 show the peaks corresponding to $^{13}CH_4$ appearing at 17 Dalton. It is important to note that injection of a sample before irradiation does not show in the chromatogram any peak at the retention time of $^{13}CH_4$.

To shed light about the main operating mechanism of the photocatalytic methanation, H_2 was replaced by dimethylaniline as sacrificial electron donor. Two possible operating mechanisms have been reported for the photocatalytic CO_2 methanation, either the so-called photothermal pathway or the photoinduced charge separation.[78] In

the photothermal mechanism, light energy is converted into local heat on the metal NPs and thus temperature increases on the NP surface promotes the thermal conversion of CO_2 and H_2 into the product.[78] This local temperature increase is undetectable by measurements of the macroscopic system due to the low RuO_x proportion. In the photocatalytic mechanism, light absorption leads to charge separation with generation of electrons in the conduction band and holes in the valence band that causes CO_2 reduction and H_2 oxidation, respectively. In the photoinduced charge separation state, the use of an electron donor better than H_2 should equally result in CO_2 conversion to methane, with an even higher reaction rate than using H_2 as reagent. On the contrary, this electron donor should not be adequate for the photothermal reaction. In the present study, dimethylaniline (0.76 V vs Ag/AgCl) was selected as electron donor.[82] The results showed that CH_4 is formed in the presence of dimethylaniline even at higher rate than in the presence of H_2 as reagent, reaching a CH_4 production rate in 5 h of 250 μmol/$g_{catalyst}^{-1}$ compared to 180 μmol/$g_{catalyst}^{-1}$ when using H_2 as reagent. This behavior is consistent with the prevalent operation of a photocatalytic mechanism.

The occurrence of photoinduced charge separation and the reaction of this photoinduced charge separated state with electron donors was additionally confirmed by photocurrent measurements. A thin film of MIP-208@RuO_x was further deposited on a transparent FTO electrode. Starting from a polarization potential of 1.6 V, the MIP-208@RuO_x electrode was submitted to a decreasing bias potential in a single electrochemical cell using tetrapropylammonium tetrafluoroborate in acetonitrile as electrolyte. The current density clearly increased at each voltage upon illumination of the photoanode with the output of a Xe lamp (Figure S18). Furthermore, the presence of methanol as electron donor increases significantly the photocurrent, indicating that this reagent is acting as sacrificial electron donor, becoming oxidized and donating electrons to the MIP-208@RuO_x in its excited state.

In summary, benefiting from a synergetic adjustment including both the preformed

Ti_8AF cluster rearrangement and the in situ linker formation that slows down the reaction, MIP-208, the first Ti-IPA MOF, was synthesized with high crystallinity and tunable scale. In its crystal structure, isostructural to CAU-10, constituted by *cis*-connected corner-sharing TiO_6 polyhedra extends along the *c*-axis resulting in a 1D helical chain inorganic building unit. Multivariate MIP-208 structures with tunable chemical environment and sizable porosity could be achieved by adopting the solid-solution mixed linker strategy. This material was proven to be the best photocatalyst for CO_2 methanation regarding activity and selectivity among all the pure MOFs, owing to its excellent stability and photoresponse. Further improvement of catalytic activity was achieved by photodeposition of RuO_x. The resulting MIP-208@RuO_x composite exhibits under the same conditions an efficiency enhancement about 20 times in comparison with that of the pure MOF. The composite catalyst displays a good stability and reusability. These results illustrate the continuous interest in the synthesis of novel Ti-MOFs that could lead to improved photocatalyst generations, suitable for the production of solar fuels and photoinduced CO_2 methanation.

EXPERIMENTAL PROCEDURES

Synthesis of MIP-208 (small scale). To a 23 mL Teflon reactor, Ti_8AF cluster solid (220 mg) was added followed by adding acetic anhydride (5 mL) and acetic acid (5 mL). The mixture was stirred at room temperature for 20 minutes before 5-NH_2-IPA (362 mg, 2 mmol) was added once. After stirring for 10 minutes, MeOH (0.5 mL) was added and the overall mixture was stirred at room temperature for another 10 minutes. Afterwards, the reaction was heated in an oven at 180 °C for 48 hours. When the reaction was cooled to room temperature, the dark yellow/light brown product was collected by filtration, washed with acetone for air dry. Yield: 330 mg (average of five parallel reactions).

Synthesis of MIP-208 (scale-up). To a 125 mL Teflon reactor, Ti_8AF cluster solid (3.5 g) was added followed by adding acetic anhydride (25 mL) and acetic acid (25 mL). The mixture was stirred at room temperature for 20 minutes before 5-NH_2-IPA (3.62 g, 20 mmol) was added once. After stirring for 10 minutes, MeOH (3.5 mL) was added and the overall mixture was stirred at room temperature for another 10 minutes. Afterwards, the reaction was heated in an oven at 180 °C for 48 hours. When the reaction was cooled to room temperature, the dark yellow/light brown product was collected by filtration, washed with acetone for air dry. Yield: 4.3 g (average of five parallel reactions).

Typical synthesis of MTV-MIP-208. To a 23 mL Teflon reactor, Ti_8AF cluster solid (220 mg) was added followed by adding acetic anhydride (5 mL) and acetic acid (5 mL). The mixture was stirred at room temperature for 20 minutes before a linker mixture of 5-NH_2-IPA (1 mmol) and the secondary IPA ligand (1 mmol) was added. After stirring for 10 minutes, MeOH (0.5 mL) was added and the overall mixture was stirred at room temperature for another 10 minutes. Afterwards, the reaction was heated in an oven at 180 °C for 48 hours. When the reaction was cooled to room temperature, the dark yellow/light brown product was collected by filtration, washed with acetone for air dry.

Photocatalytic methanation tests. The photocatalytic CO_2 methanation experiments were carried out using a quartz photoreactor (51 mL) equipped with a heating mantle to control the desired temperature. In a typical experiment the powder photocatalyst (15 mg) is placed as a

bed in the reactor, and then the system purged first with H_2 and later with CO_2 until a ratio of 4 to 1 is obtained. Subsequently, the photoreactor is heated at 200 ºC, and then the photocatalyst was irradiated using a Xe lamp (300 W) or a solar simulator. At the desired reaction time an aliquot was sampled from the photoreactor and analyzed in an Agilent 490 MicroGC equipped with two channels and thermal conductivity detectors. One channel equipped with a MolSieve 5Å column allows analysis of H_2, O_2, N_2 and CO, while the other channel equipped with a Pore Plot Q column allows determining CO_2, CH_4 and short chain hydrocarbons. Quantification was performed using calibration plots employing commercially available gas mixtures.

X-ray crystallographic data. The X-ray crystallographic data for MIP-208 have been deposited at the Cambridge Crystallographic Data Centre (CCDC), under deposition number CCDC 1989406. These data can be obtained free of charge from the CCDC database via www.ccdc.cam.ac.uk. All other relevant data supporting the findings of this study are available from the corresponding authors on request.

ACKNOWLEDGEMENTS

CMC is grateful for financial support from the Institut Universitaire de France (IUF) and the Paris Ile-de- France Region – DIM "Respore". S.N. thanks financial support by the Fundación Ramón Areces (XVIII Concurso Nacional para la Adjudicación de Ayudas a la Investigación en Ciencias de la Vida y de la Materia, 2016), Ministerio de Ciencia, Innovación y Universidades RTI2018-099482-A-I00 project and Generalitat Valenciana grupos de investigación consolidables 2019 (AICO/2019/214) project. H.G. thanks financial support to the Spanish Ministry of Science and Innovation (Severo Ochoa and RTI2018-098237-CO2-1) and Generalitat Valenciana (Prometeo2017/083).

AUTHOR CONTRIBUTIONS

Conceptualization, S.W., C.S. S.N. and H.G.; Investigation, S.W., M.C-A., S.N., C-C.C., A.T., J.M., C.M.-C., W.S., H.G., and C.S.; Writing – Original Draft, S.W.; Writing – Review &

Editing, S.W., S.N., A.T., C.M.-C., H.G., and C.S. Supervision, H.G., and C.S.

DECLARATION OF INTERESTS

The authors declare no competing interests.

REFERENCES

1. Dhakshinamoorthy A., Li Z., and Garcia H. (2018). Catalysis and photocatalysis by metal organic frameworks. Chemical Society Reviews *47*, 8134-8172.

2. Chen L., and Xu Q. (2019). Metal-Organic Framework Composites for Catalysis. Matter *1*, 57-89.

3. García H., and Navalón S. (2018). In Metal-Organic Frameworks: Applications in Separations and Catalysis (Wiley-VCH Verlag GmbH & Co. KGaA).

4. Yeung H. H.-M., Li W., Saines P. J., Köster T. K. J., Grey C. P., and Cheetham A. K. (2013). Ligand-Directed Control over Crystal Structures of Inorganic–Organic Frameworks and Formation of Solid Solutions. Angewandte Chemie International Edition *52*, 5544-5547.

5. Lu W., Wei Z., Gu Z.-Y., Liu T.-F., Park J., Park J., et al. (2014). Tuning the structure and function of metal–organic frameworks via linker design. Chemical Society Reviews *43*, 5561-5593.

6. Desai A. V., Sharma S., Let S., and Ghosh S. K. (2019). N-donor linker based metal-organic frameworks (MOFs): Advancement and prospects as functional materials. Coord Chem Rev *395*, 146-192.

7. Zhang H., Zou R., and Zhao Y. (2015). Macrocycle-based metal-organic frameworks.

Coord Chem Rev *292*, 74-90.

8. He Y., Li B., O'Keeffe M., and Chen B. (2014). Multifunctional metal–organic frameworks constructed from meta-benzenedicarboxylate units. Chemical Society Reviews *43*, 5618-5656.

9. Kuppler R. J., Timmons D. J., Fang Q.-R., Li J.-R., Makal T. A., Young M. D., et al. (2009). Potential applications of metal-organic frameworks. Coord Chem Rev *253*, 3042-3066.

10. Czaja A. U., Trukhan N., and Müller U. (2009). Industrial applications of metal–organic frameworks. Chemical Society Reviews *38*, 1284-1293.

11. Silva P., Vilela S. M. F., Tomé J. P. C., and Almeida Paz F. A. (2015). Multifunctional metal–organic frameworks: from academia to industrial applications. Chemical Society Reviews *44*, 6774-6803.

12. Ren J., Dyosiba X., Musyoka N. M., Langmi H. W., Mathe M., and Liao S. (2017). Review on the current practices and efforts towards pilot-scale production of metal-organic frameworks (MOFs). Coord Chem Rev *352*, 187-219.

13. Hillesheim P. M. L. F. K. T. W. E. R. J. N. B. W. (2007). Phthalic Acid and Derivatives. In Ullmann's Encyclopedia of Industrial Chemistry.

14. Sheehan R. J. (2011). Terephthalic Acid, Dimethyl Terephthalate. In Ullmann's Encyclopedia of Industrial Chemistry.

15. Ohtani M., Takase K., Wang P., Higashi K., Ueno K., Yasuda N., et al. (2016). Water-triggered macroscopic structural transformation of a metal–organic framework. CrystEngComm *18*, 1866-1870.

16. Padmanabhan M., Joseph K. C., Puranik V. G., Huang X., and Li J. (2007). An unprecedented two-dimensional polymeric [Zn(OOC–C6H4–COO)2]n2 − [+H3N – (CH2)3 –

NH3+]n system bearing one-dimensional chain of zinc(II) bis(phthalate) dianions held by propane-1,3-diammonium cations: Crystal structure, thermal and fluorescent properties. Solid State Sciences *9*, 491-495.

17. Reinsch H., De Vos D., and Stock N. (2013). Structure and Properties of [Al4(OH)8(o-C6H4(CO2)2)2]·H2O, a Layered Aluminum Phthalate. Zeitschrift für anorganische und allgemeine Chemie *639*, 2785-2789.

18. Li H., Davis C. E., Groy T. L., Kelley D. G., and Yaghi O. M. (1998). Coordinatively Unsaturated Metal Centers in the Extended Porous Framework of Zn3(BDC)3·6CH3OH (BDC = 1,4-Benzenedicarboxylate). Journal of the American Chemical Society *120*, 2186-2187.

19. Banerjee D., and Parise J. B. (2011). Recent Advances in s-Block Metal Carboxylate Networks. Cryst Growth Des *11*, 4704-4720.

20. Pagis C., Ferbinteanu M., Rothenberg G., and Tanase S. (2016). Lanthanide-Based Metal Organic Frameworks: Synthetic Strategies and Catalytic Applications. ACS Catalysis *6*, 6063-6072.

21. Aguirre-Díaz L. M., Reinares-Fisac D., Iglesias M., Gutiérrez-Puebla E., Gándara F., Snejko N., et al. (2017). Group 13th metal-organic frameworks and their role in heterogeneous catalysis. Coord Chem Rev *335*, 1-27.

22. Kang M., Luo D., Deng Y., Li R., and Lin Z. (2014). Solvothermal synthesis and characterization of new calcium carboxylates based on cluster- and rod-like building blocks. Inorganic Chemistry Communications *47*, 52-55.

23. Bourne S. A., Lu J., Mondal A., Moulton B., and Zaworotko M. J. (2001). Self-Assembly of Nanometer-Scale Secondary Building Units into an Undulating Two-Dimensional Network with

Two Types of Hydrophobic Cavity. Angewandte Chemie International Edition *40*, 2111-2113.

24. Vodak D. T., Braun M. E., Kim J., Eddaoudi M., and Yaghi O. M. (2001). Metal–organic frameworks constructed from pentagonal antiprismatic and cuboctahedral secondary building units. Chemical Communications, 2534-2535.

25. Barthelet K., Riou D., and Férey G. (2002). [VIII(H2O)]3O(O2CC6H4CO2)3·(Cl, 9H2O) (MIL-59): a rare example of vanadocarboxylate with a magnetically frustrated three-dimensional hybrid framework. Chemical Communications, 1492-1493.

26. Qazvini O. T., Babarao R., Shi Z.-L., Zhang Y.-B., and Telfer S. G. (2019). A Robust Ethane-Trapping Metal–Organic Framework with a High Capacity for Ethylene Purification. Journal of the American Chemical Society *141*, 5014-5020.

27. Kim J.-Y., Norquist A. J., and O'Hare D. (2003). Incorporation of uranium(vi) into metal–organic framework solids, [UO2(C4H4O4)]·H2O, [UO2F(C5H6O4)]·2H2O, and [(UO2)1.5(C8H4O4)2]2[(CH3)2NCOH2]·H2O. Dalton Transactions, 2813-2814.

28. Wang G., Song T., Fan Y., Xu J., Wang M., Zhang H., et al. (2010). [Y2(H2O)(BDC)3(DMF)]·(DMF)3: A rare 2-D (42.6)(45.6)2(48.62)(49.65.8) net with multi-helical-array and opened windows. Inorganic Chemistry Communications *13*, 502-505.

29. Mihalcea I., Henry N., Clavier N., Dacheux N., and Loiseau T. (2011). Occurence of an Octanuclear Motif of Uranyl Isophthalate with Cation–Cation Interactions through Edge-Sharing Connection Mode. Inorganic Chemistry *50*, 6243-6249.

30. Vougo-Zanda M., Wang X., and Jacobson A. J. (2007). Influence of Ligand Geometry on the Formation of In−O Chains in Metal-Oxide Organic Frameworks (MOOFs). Inorganic Chemistry *46*, 8819-8824.

31. Bu F., and Xiao S.-J. (2010). A 4-connected anionic metal–organic nanotube constructed from indium isophthalate. CrystEngComm *12*, 3385-3387.

32. Panda T., Kundu T., and Banerjee R. (2013). Structural isomerism leading to variable proton conductivity in indium(iii) isophthalic acid based frameworks. Chemical Communications *49*, 6197-6199.

33. Chen P.-K., Che Y.-X., Zheng J.-M., and Batten S. R. (2007). Heteropolynuclear Metamagnet Showing Spin Canting and Single-Crystal to Single-Crystal Phase Transformation. Chemistry of Materials *19*, 2162-2167.

34. Zhang L., Qin Y.-Y., Li Z.-J., Lin Q.-P., Cheng J.-K., Zhang J., et al. (2008). Topology Analysis and Nonlinear-Optical-Active Properties of Luminescent Metal−Organic Framework Materials Based on Zinc/Lead Isophthalates. Inorganic Chemistry *47*, 8286-8293.

35. Zhang J.-P., Ghosh S. K., Lin J.-B., and Kitagawa S. (2009). New Heterometallic Carboxylate Frameworks: Synthesis, Structure, Robustness, Flexibility, and Porosity. Inorganic Chemistry *48*, 7970-7976.

36. McCormick L. J., Morris S. A., Slawin A. M. Z., Teat S. J., and Morris R. E. (2016). Coordination Polymers of 5-Alkoxy Isophthalic Acids. Cryst Growth Des *16*, 5771-5780.

37. Chen J., Li C.-P., and Du M. (2011). Substituent effect of R-isophthalates (R = –H, –CH3, –OCH3, –tBu, –OH, and –NO2) on the construction of CdII coordination polymers incorporating a dipyridyl tecton 2,5-bis(3-pyridyl)-1,3,4-oxadiazole. CrystEngComm *13*, 1885-1893.

38. Du M., Zhang Z.-H., You Y.-P., and Zhao X.-J. (2008). R-Isophthalate (R = –H, –NO2, and –COOH) as modular building blocks for mixed-ligand coordination polymers incorporated with a versatile connector 4-amino-3,5-bis(3-pyridyl)-1,2,4-triazole. CrystEngComm *10*, 306-321.

39. Chen L., Ye J.-W., Wang H.-P., Pan M., Yin S.-Y., Wei Z.-W., et al. (2017). Ultrafast water sensing and thermal imaging by a metal-organic framework with switchable luminescence. Nat Commun *8*, 15985.

40. Yuan S., Qin J.-S., Lollar C. T., and Zhou H.-C. (2018). Stable Metal–Organic Frameworks with Group 4 Metals: Current Status and Trends. ACS Central Sci *4*, 440-450.

41. Rieth A. J., Wright A. M., and Dincă M. (2019). Kinetic stability of metal–organic frameworks for corrosive and coordinating gas capture. Nat Rev Mater.

42. Dhakshinamoorthy A., Asiri A. M., and García H. (2016). Metal–Organic Framework (MOF) Compounds: Photocatalysts for Redox Reactions and Solar Fuel Production. Angewandte Chemie International Edition *55*, 5414-5445.

43. Alvaro M., Carbonell E., Ferrer B., Llabrés i Xamena F. X., and Garcia H. (2007). Semiconductor Behavior of a Metal-Organic Framework (MOF). Chemistry – A European Journal *13*, 5106-5112.

44. Nasalevich M. A., Goesten M. G., Savenije T. J., Kapteijn F., and Gascon J. (2013). Enhancing optical absorption of metal–organic frameworks for improved visible light photocatalysis. Chemical Communications *49*, 10575-10577.

45. Zhu J. J., Li P. Z., Guo W. H., Zhao Y. L., and Zou R. Q. (2018). Titanium-based metal-organic frameworks for photocatalytic applications. Coord Chem Rev *359*, 80-101.

46. Benoit V., Pillai R. S., Orsi A., Normand P., Jobic H., Nouar F., et al. (2016). MIL-91(Ti), a small pore metal–organic framework which fulfils several criteria: an upscaled green synthesis, excellent water stability, high CO2 selectivity and fast CO2 transport. Journal of Materials Chemistry A *4*, 1383-1389.

47. Sun Y., Liu Y., Caro J., Guo X., Song C., and Liu Y. (2018). In-Plane Epitaxial Growth of Highly c-Oriented NH2-MIL-125(Ti) Membranes with Superior H2/CO2 Selectivity. Angew ChemInt Ed *57*, 16088-16093.

48. Wahiduzzaman M., Wang S., Schnee J., Vimont A., Ortiz V., Yot P. G., et al. (2019). A High Proton Conductive Hydrogen-Sulfate Decorated Titanium Carboxylate Metal−Organic Framework. ACS Sustainable Chemistry & Engineering *7*, 5776-5783.

49. Pinto R. V., Wang S., Tavares S. R., Pires J., Antunes F., Vimont A., et al. Tuning Cellular Biological Functions Through the Controlled Release of NO from a Porous Ti-MOF. Angewandte Chemie International Edition *n/a*.

50. Assi H., Mouchaham G., Steunou N., Devic T., and Serre C. (2017). Titanium coordination compounds: from discrete metal complexes to metal–organic frameworks. Chem Soc Rev *46*, 3431-3452.

51. Tachikawa T., Tojo S., Fujitsuka M., Sekino T., and Majima T. (2006). Photoinduced Charge Separation in Titania Nanotubes. The Journal of Physical Chemistry B *110*, 14055-14059.

52. Wang S., Kitao T., Guillou N., Wahiduzzaman M., Martineau-Corcos C., Nouar F., et al. (2018). A phase transformable ultrastable titanium-carboxylate framework for photoconduction. Nat Commun *9*, 1660.

53. Serre C., Groves J. A., Lightfoot P., Slawin A. M. Z., Wright P. A., Stock N., et al. (2006). Synthesis, Structure and Properties of Related MicroporousN,N‘-Piperazinebismethylenephosphonates of Aluminum and Titanium. Chem Mat *18*, 1451-1457.

54. Li C., Xu H., Gao J., Du W., Shangguan L., Zhang X., et al. (2019). Tunable titanium metal–organic frameworks with infinite 1D Ti–O rods for efficient visible-light-driven photocatalytic H2 evolution. J Mater Chem A *7*, 11928-11933.

55. Keum Y., Park S., Chen Y.-P., and Park J. (2018). Titanium-Carboxylate Metal-Organic Framework Based on an Unprecedented Ti-Oxo Chain Cluster. Angew ChemInt Ed *57*, 14852-14856.

56. Yuan S., Liu T.-F., Feng D., Tian J., Wang K., Qin J., et al. (2015). A single crystalline porphyrinic titanium metal–organic framework. Chem Sci *6*, 3926-3930.

57. Padial N. M., Castells-Gil J., Almora-Barrios N., Romero-Angel M., da Silva I., Barawi M., et al. (2019). Hydroxamate Titanium–Organic Frameworks and the Effect of Siderophore-Type Linkers over Their Photocatalytic Activity. Journal of the American Chemical Society *141*, 13124-13133.

58. Wang S., Reinsch H., Heymans N., Wahiduzzaman M., Martineau-Corcos C., De Weireld G., et al. (2020). Toward a Rational Design of Titanium Metal-Organic Frameworks. Matter *2*, 440-450.

59. Hendon C. H., Tiana D., Fontecave M., Sanchez C., D'Arras L., Sassoye C., et al. (2013). Engineering the optical response of the titanium-MIL-125 metal-organic framework through ligand functionalization. J Am Chem Soc *135*, 10942-10945.

60. Fu Y., Sun D., Chen Y., Huang R., Ding Z., Fu X., et al. (2012). An Amine-Functionalized Titanium Metal–Organic Framework Photocatalyst with Visible-Light-Induced Activity for CO2 Reduction. Angew ChemInt Ed *51*, 3364-3367.

61. Duran D., Couster S. L., Desjardins K., Delmotte A., Fox G., Meijers R., et al. (2013).

PROXIMA 2A – A New Fully Tunable Micro-focus Beamline for Macromolecular Crystallography. J Phys Conf Ser *425*, 012005.

62. Reinsch H., van der Veen M. A., Gil B., Marszalek B., Verbiest T., de Vos D., et al. (2013). Structures, Sorption Characteristics, and Nonlinear Optical Properties of a New Series of Highly Stable Aluminum MOFs. Chemistry of Materials *25*, 17-26.

63. Férey G., and Serre C. (2009). Large breathing effects in three-dimensional porous hybrid matter: facts, analyses, rules and consequences. Chemical Society Reviews *38*, 1380-1399.

64. Férey G. (2016). Giant flexibility of crystallized organic–inorganic porous solids: facts, reasons, effects and applications. New J Chem *40*, 3950-3967.

65. Leshuk T., Parviz R., Everett P., Krishnakumar H., Varin R. A., and Gu F. (2013). Photocatalytic Activity of Hydrogenated TiO2. ACS Appl Mater Interfaces *5*, 1892-1895.

66. Chen X., Liu L., and Huang F. (2015). Black titanium dioxide (TiO2) nanomaterials. Chemical Society Reviews *44*, 1861-1885.

67. Liu L., and Chen X. (2014). Titanium Dioxide Nanomaterials: Self-Structural Modifications. Chemical Reviews *114*, 9890-9918.

68. Reinsch H., Waitschat S., and Stock N. (2013). Mixed-linker MOFs with CAU-10 structure: synthesis and gas sorption characteristics. Dalton Transactions *42*, 4840-4847.

69. Deng H., Doonan C. J., Furukawa H., Ferreira R. B., Towne J., Knobler C. B., et al. (2010). Multiple Functional Groups of Varying Ratios in Metal-Organic Frameworks. Science *327*, 846-850.

70. Foo M. L., Matsuda R., and Kitagawa S. (2014). Functional Hybrid Porous Coordination Polymers. Chemistry of Materials *26*, 310-322.

71. Helal A., Yamani Z. H., Cordova K. E., and Yaghi O. M. (2017). Multivariate metal-organic frameworks. National Science Review *4*, 296-298.

72. Ding M., Flaig R. W., Jiang H.-L., and Yaghi O. M. (2019). Carbon capture and conversion using metal–organic frameworks and MOF-based materials. Chemical Society Reviews *48*, 2783-2828.

73. Li R., Hu J., Deng M., Wang H., Wang X., Hu Y., et al. (2014). Integration of an Inorganic Semiconductor with a Metal–Organic Framework: A Platform for Enhanced Gaseous Photocatalytic Reactions. Advanced Materials *26*, 4783-4788.

74. Cabrero-Antonino M., Remiro-Buenamañana S., Souto M., García-Valdivia A. A., Choquesillo-Lazarte D., Navalón S., et al. (2019). Design of cost-efficient and photocatalytically active Zn-based MOFs decorated with Cu2O nanoparticles for CO2 methanation. Chemical Communications *55*, 10932-10935.

75. Ulmer U., Dingle T., Duchesne P. N., Morris R. H., Tavasoli A., Wood T., et al. (2019). Fundamentals and applications of photocatalytic CO2 methanation. Nat Commun *10*, 3169.

76. Younas M., Loong Kong L., Bashir M. J. K., Nadeem H., Shehzad A., and Sethupathi S. (2016). Recent Advancements, Fundamental Challenges, and Opportunities in Catalytic Methanation of CO2. Energy & Fuels *30*, 8815-8831.

77. Mateo D., Albero J., and García H. (2019). Titanium-Perovskite-Supported RuO2 Nanoparticles for Photocatalytic CO2 Methanation. Joule *3*, 1949-1962.

78. Wenderich K., and Mul G. (2016). Methods, Mechanism, and Applications of Photodeposition in Photocatalysis: A Review. Chemical Reviews *116*, 14587-14619.

79. Giang T. P. L., Tran T. N. M., and Le X. T. (2012). Preparation and characterization of

titanium dioxide nanotube array supported hydrated ruthenium oxide catalysts. Advances in Natural Sciences: Nanoscience and Nanotechnology *3*, 015008.

80. Morgan D. J. (2015). Resolving ruthenium: XPS studies of common ruthenium materials. Surface and Interface Analysis *47*, 1072-1079.

81. Mateo D., Santiago-Portillo A., Albero J., Navalon S., Alvaro M., and Garcia H. (2019). Long-Term Photostability in Terephthalate Metal-Organic Frameworks. Angewandte Chemie-International Edition *58*, 17843-17848.

82. Mateo D., Albero J., and García H. (2018). Graphene supported NiO/Ni nanoparticles as efficient photocatalyst for gas phase CO2 reduction with hydrogen. Applied Catalysis B: Environmental *224*, 563-571.